Available online at www.sciencedirect.com
SCIENCE DIRECT®
Journal of Nuclear Materials 348 (2006) 283–293
journal of nuclear materials
www.elsevier.com/locate/jnucmat

Velocity distribution of helium and neon atoms released from graphite and tungsten limiters in TEXTOR

P. Lindner [a,*], M. Brix [b], Ph. Mertens [b], A. Pospieszczyk [b], U. Samm [b], B. Schweer [b], B. Unterberg [b]

[a] Institut für Plasmaforschung, Universität Stuttgart, Pfaffenwaldring 31, D-70569 Stuttgart, Germany
[b] Institut für Plasmaphysik, Forschungszentrum Jülich GmbH, EURATOM Association, D-52425 Jülich, Germany

Received 20 May 2005; accepted 28 September 2005

Abstract

The release mechanisms of noble gases from plasma-facing components were observed spectroscopically in the TEXTOR plasma boundary by determining the velocity distribution from Doppler broadening. For the first time, three different mechanisms for helium and neon release from graphite and tungsten limiters could be distinguished quantitatively in a tokamak: thermal desorption, ion-induced desorption and particle reflection. Under the assumption that the thermal desorption follows a Maxwellian velocity distribution, the ion-induced desorption can be expressed by a Thompson velocity distribution. Calculating the particle reflection by the Monte-Carlo code TRIM, these processes could be separated in the measured velocity distribution.

PACS: 52.40.H

1. Introduction

Impurity release and transport is one of the key problems on the way to controlled nuclear fusion [1–3]. In addition to particle transport in the plasma core, processes occurring at the plasma edge, namely the penetration of impurity neutrals released from the plasma-facing components into the confined plasma, have a direct and significant influence on the central impurity density. Helium and neon are impurities of special interest in this context: helium is the product of the DT-fusion process and, therefore unavoidably present in a burning plasma, and neon is representative of candidates in the concept of power exhaust from a radiating plasma mantle in a next step device like ITER [4]. Carbon and tungsten are presently foreseen as plasma-facing components in ITER. As a consequence, there is an urgent need to investigate the plasma surface interaction of these species and their penetration into the confined plasma volume.

The velocity distribution of helium and neon atoms has been determined in TEXTOR from the Doppler shift of atomic line emission. For the first time three different release mechanisms for helium and neon from carbon and tungsten limiters could

* Corresponding author.
E-mail address: lindner@ipf.uni-stuttgart.de (P. Lindner).

0022-3115/$ - see front matter
doi:10.1016/j.jnucmat.2005.09.020

be distinguished in a tokamak: thermal desorption, ion-induced desorption and particle reflection. Under the assumption that the thermal desorption can be described by a Maxwellian velocity distribution [5], the ion induced desorption profile can be approximated by a Thompson velocity distribution [6], which is normally reserved for physical sputtering. Calculating the particle reflection by the Monte-Carlo code TRIM [7], these three processes present in the measured velocity distribution could be separated.

2. Experimental set-up

The experiments have been performed on the tokamak TEXTOR with a major radius of $R = 1.75$ m and a minor radius of $a = 0.46$ m, a toroidal magnetic field $B_T = 2.25$ T and a plasma current $I_P = 350$ kA. The plasma was additionally heated by neutral beam co-injection ($P_{NBI} = 1.3$ MW) and the line-averaged central density was varied between 2.5×10^{19} m^{-3} and 5×10^{19} m^{-3}. Neon feedbacked seeding was applied to keep the fraction of radiated power with respect to the input power constant at various levels. The measurements shown below have been carried out using test limiters made of two different materials (graphite and tungsten), which were inserted into the vacuum vessel by the limiter lock system at the bottom of the torus [8]. The shape of the test limiter has a spherical sector with a radius of 70 mm, a bottom length of 120 mm and a bottom width of 80 mm. The limiters were observed from the top of TEXTOR and, using another port, tangentially. The test limiter and the map of the observation are shown in Fig. 1(a). Fig. 1(b) shows the poloidal cross-section with the tangential and the top observation. The Doppler broadened intensity profile of the line emission from neutral helium and neon has been measured from the top by guiding the emitted light with fibers to a high resolution spectrometer ($\lambda/\Delta\lambda = 2 \times 10^5$). The spectrometer is in a Littrow configuration with an echelle grating of 220 mm width and 75 lines/mm. The measurements of the He I line at $\lambda = 728.135$ nm ($3s^1S - 2p^1P^0$) were performed in the 33rd order and those for Ne I at $\lambda = 585.249$ nm $3p'[1/2]_{J=0} - 3s'[1/2]_{J=1}$ in the 42nd order. In addition to the Doppler broadening, the line shape is influenced by the Zeeman-effect. For both observed lines, the σ-component ($\Delta M = \pm 1$) of the Zeeman pattern has been filtered out by using a polarizer. Fig. 2 shows the intensity profile of the Ne I line in front of a graphite limiter with and without polarizer. The intensity profile measured with a polarizer still shows small σ-components of the Zeeman pattern, which may originate from the diffuse light reflection on the rough surface of the limiter. Neon or helium glow discharges through a Plücker tube were used for an accurate in-situ determination of the reference wavelength λ_0. The remaining Doppler shift $\Delta\lambda = \lambda_0 v/c$ of the line emitted by an atom moving with the velocity v in the direction of the observer allows the deduction of the velocity distribution $f(v)dv$ from the Doppler shifted and

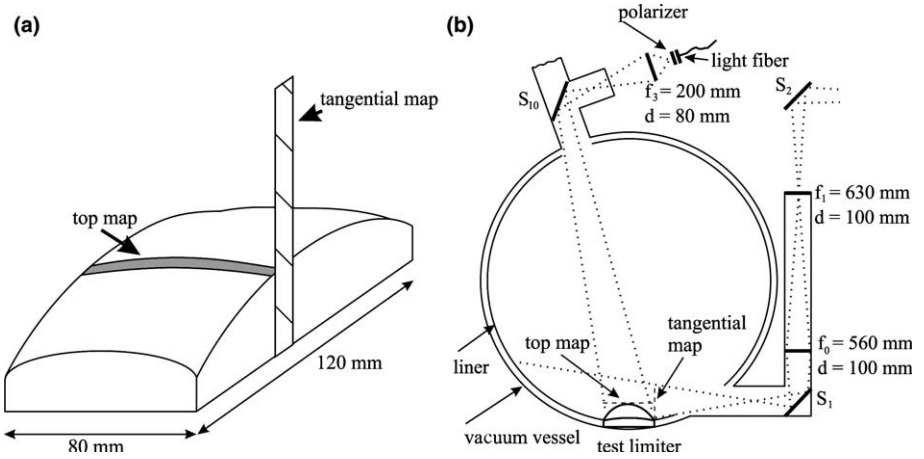

Fig. 1. (a) Test limiter sketch with the top and tangential map of the fiber and the spectrometer slit. (b) The poloidal cross-section on TEXTOR with the observation geometries. The upper observation direction is used to determine the Doppler intensity profiles and the lower tangential observation direction is used to measure the radial intensity distribution.

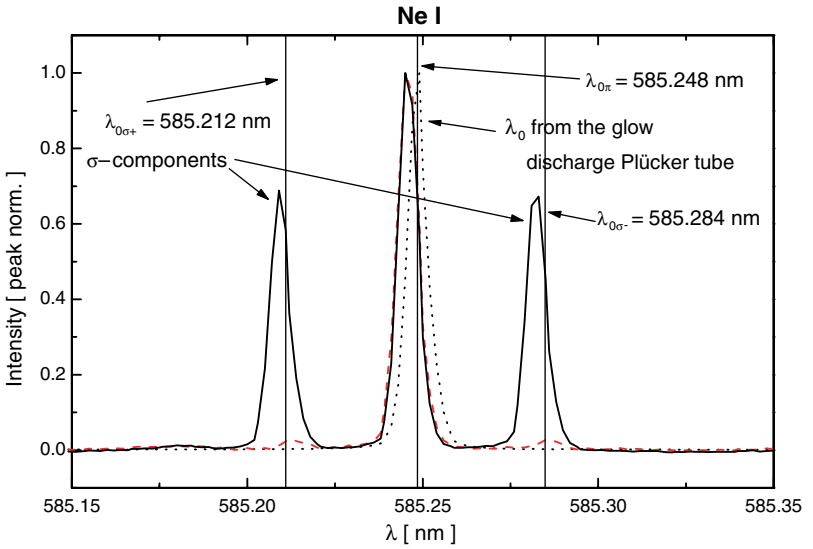

Fig. 2. Intensity profile from a TEXTOR discharge of Ne I at $\lambda = 585.249$ nm $3p'[1/2]_{J=0} - 3s'[1/2]_{J=1}$ at the Graphite limiter, with (dashed line) and without (solid line) polarizer. The dotted line is measured in a glow discharge of a Plücker tube to determine the reference wavelength λ_0.

broadened intensity profile. Atoms with a velocity distribution $f(v)$ lead to a line shape which can be described by

$$L(\Delta\lambda)\mathrm{d}\lambda = f(v)\mathrm{d}v = (c/\lambda_0)f(c\Delta\lambda/\lambda_0)\mathrm{d}\lambda\,. \qquad (1)$$

The integration of $L(\Delta\lambda)$ over the line of sight corresponds to the measured intensity $I(\Delta\lambda)$. Since the fast atoms travel a longer path than the slow ones before they are ionized, the line of sight integrated profile $I(\Delta\lambda)$ is in the first approximation [9,10] not proportional to the local velocity but it is proportional to the velocity distribution of the atomic flux $\Gamma(v = c\Delta\lambda/\lambda_0)$.

The limiter is observed tangentially using a Czerny–Turner mounted spectrometer (Acton Research SpectraPro 500) equipped with an intensified CCD camera as detector which yields spectra of radially resolved line emission (see Fig. 1) in the wavelength range $\lambda = 200$–800 nm. The spectrometer was used with a grating of 1200 lines/mm and a resolution of $\lambda/\Delta\lambda = 2\times10^4$. An example of the Ne I line at $\lambda = 585.24$ nm is shown in Fig. 3. The profiles of the electron temperature (T_e) and density (n_e), which are obtained by means of thermal helium beam diagnostic [11,12], govern the plasma sheath and consequently the ion energy distribution, the ion angle of incidence, the excitation and the ionization processes of atoms in front of the limiter.

3. Experimental results

Fig. 4 shows the measured velocity distribution of helium and neon atoms released from a graphite and from a tungsten limiter in two different target plasmas. The measured intensity distribution of He I on the graphite limiter shows a pronounced maximum at 3×10^3 m/s (0.2 eV) with a small amount of fast atoms which decreases with increasing velocities. A second maximum at 2×10^4 m/s is the result of light reflection on the limiter surface which leads to insufficient elimination of the σ-component of the Zeeman pattern. With decreasing electron temperature the main maximum is shifted towards higher velocities and a slight increase of the intensity distribution at higher velocities is observed (Fig. 4(a)). With the change of limiter material from graphite to tungsten, a shift of the maximum and a significantly larger fraction of fast atoms are detected (Fig. 4(b)).

The intensity distribution of Ne I shows a more pronounced behavior than He I. With a decreasing electron temperature an increase of the fast part of the intensity distribution is observed. The velocity 1×10^3 m/s (0.1 eV), where the velocity distribution peaks, remains within the accuracy of measurement unchanged (Fig. 4(c)). As in the case of helium, more fast neon atoms are released from the tungsten limiter than from the carbon limiter. The second maximum at 1.7×10^4 m/s has its

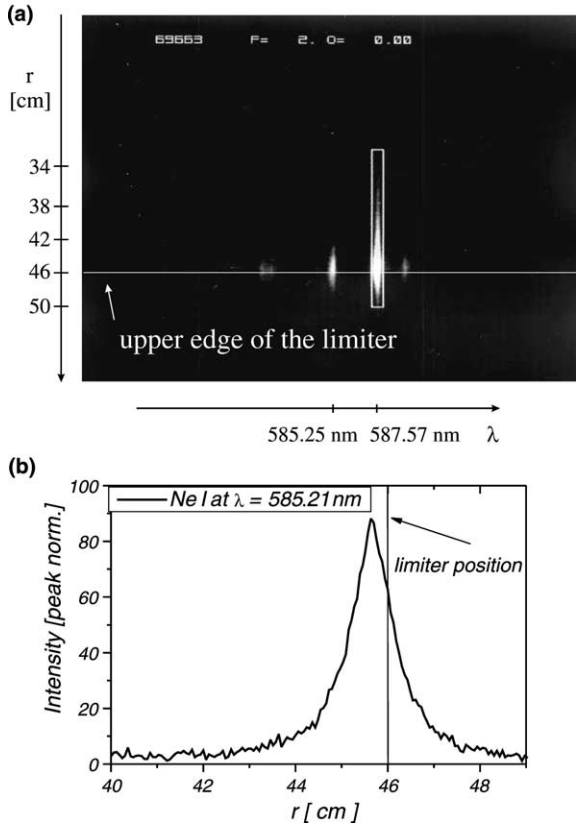

Fig. 3. (a) 2D snap shot of the tangential observation. The horizontal axis shows the wavelength and the vertical one the spatial resolution which illustrates the radial distribution of the intensity. The horizontal line marks the position of the test limiter. The box illustrates the chosen atomic line which will be horizontally integrated. (b) An example of the measured radial intensity profile of Ne I at $\lambda = 585.21$ nm ($\sigma+$).

origin in the light reflection on the limiter surface. This artifact is even more pronounced on tungsten due to the higher light reflection coefficient of a tungsten surface compared to a graphite surface (Fig. 4(d)).

A semi-logarithmic plot of the helium velocity distribution from the graphite limiter (Fig. 5(a)) at low energies indicates that the intensity distribution can be described by a shifted Maxwellian distribution (Fig. 7). This shape has been observed for all combinations of recycling gases and limiter materials which are reported here. The double logarithmic diagram (Fig. 5(b)) of helium on the graphite limiter shows a $E^{-1.8}$ dependence in the intermediate energy range. The analysis of more than 50 intensity distributions has revealed an average exponent of -2 ± 0.5. We have found that the accuracy of the determined exponent strongly depends on the background subtraction.

The radially resolved intensity profiles of He I as well as of Ne I depend only slightly on the electron temperature, but are strongly influenced by the choice of the limiter material. An example of a radial intensity profile at $\lambda = 587.57$ nm of helium on the graphite limiter and of helium on the tungsten limiter is shown in Fig. 6. As it can be seen, the intensity of helium is higher at smaller radii in the tungsten limiter experiments compared to the graphite limiter experiments, which had similar local plasma conditions. From this, one can conclude that helium originating from a tungsten surface penetrates deeper into the confined plasma than it would originate from graphite.

4. Discussion

The experimental results show that the intensity distributions of He I and Ne I have dominant maxima at low velocities which are only slightly dependent on the plasma parameter and the choice of the limiter material. The intensity profile at low velocities can be described by a Maxwellian distribution.

In the intermediate energy (velocity) range (1–2 eV) an E^{-2} dependence is observed.

The high velocity (energy) part of the intensity distribution increases with decreasing electron temperature and with the change of limiter material from graphite to tungsten.

Taking these three results into account, the intensity distribution of helium and neon will be governed by the following release mechanism from the limiter surface:

- thermal desorption,
- ion-induced desorption,
- particle reflection at the limiter surface.

The velocities of the thermally desorbed atoms are described by a Maxwellian distribution [5], the velocities of the atoms released by ion-induced desorption are described by the Thompson distribution [6] and the particle reflection is numerically simulated by the TRIM code [7].

One has to take into account that the measured intensity is proportional to the impurity flux [9,10] and that the velocity distribution will be influenced by the geometry of sight [14]. Atoms originating outside the observation volume may move into it

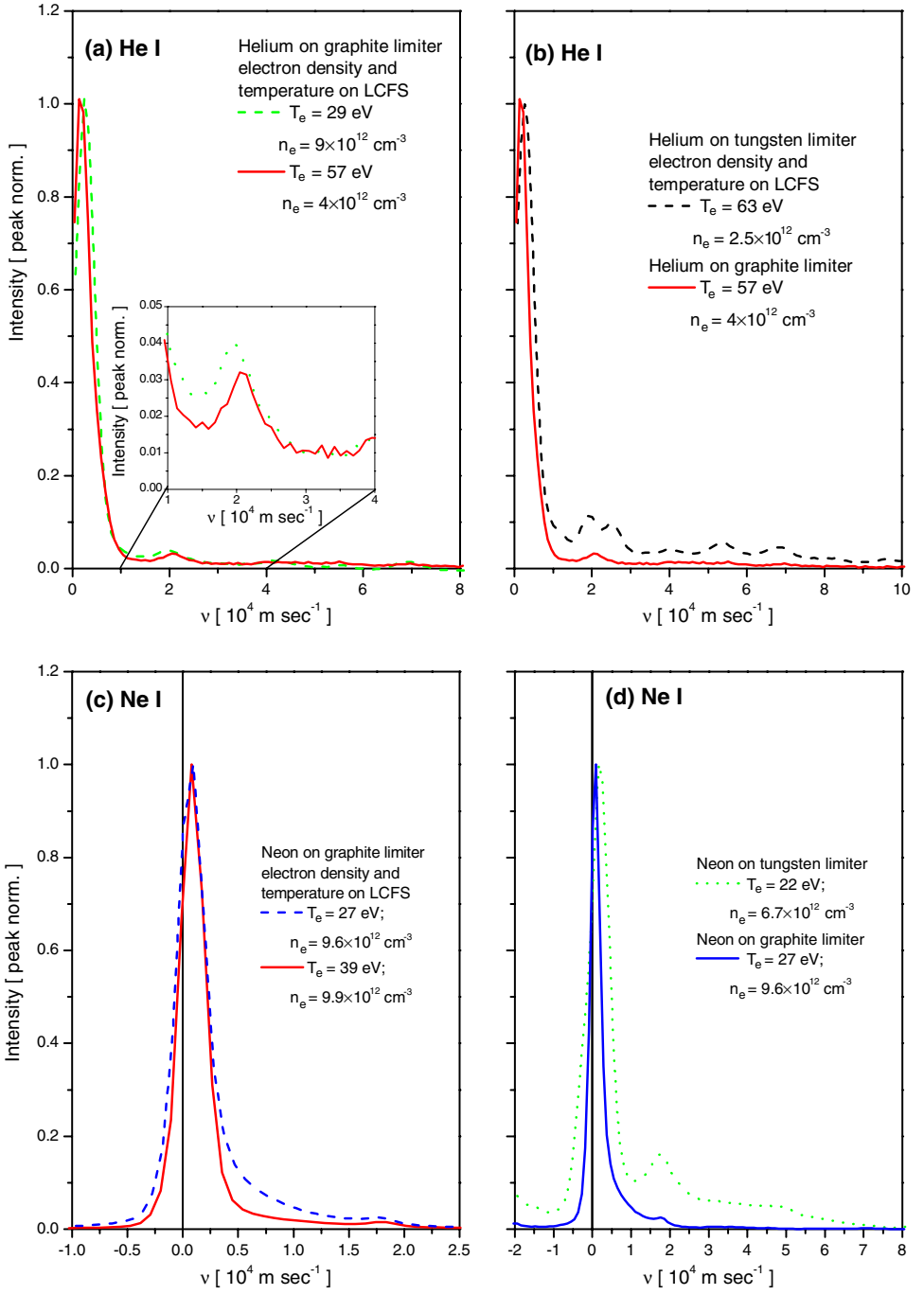

Fig. 4. (a) The Doppler-broadening-dominated intensity distribution of He I on a graphite limiter for different plasma parameters. (b) The comparison of the intensity profiles of He I on tungsten and on graphite limiter shows an increasing part of fast atoms. (c) The intensity distribution of Ne I on a graphite limiter for a cold and a hot plasma boundary in TEXTOR. (d) Ne I Doppler broadening dominated profile observed for different limiter materials (top view).

and emit a photon. The probability of reaching the observation volume increases with their velocities. Infrared measurements [9] on the limiter exhibited two hot spots with radii, R, of 20 mm. Spectroscopic measurements show the highest intensities in these regions. Therefore it is very likely that most of the recycling takes place in front of the hot spots.

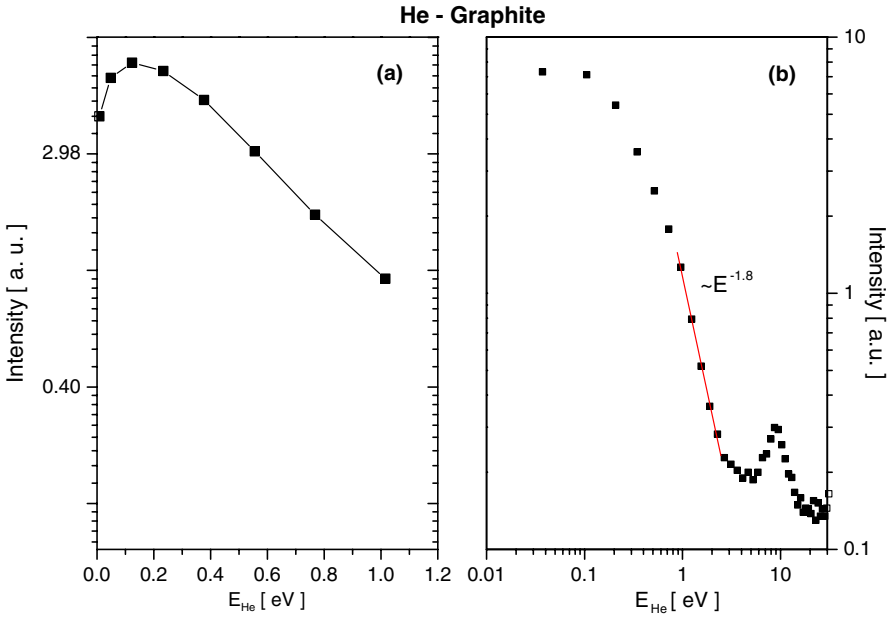

Fig. 5. Intensity distribution versus energy of the He I atoms in a semi logarithmic plot (top view).

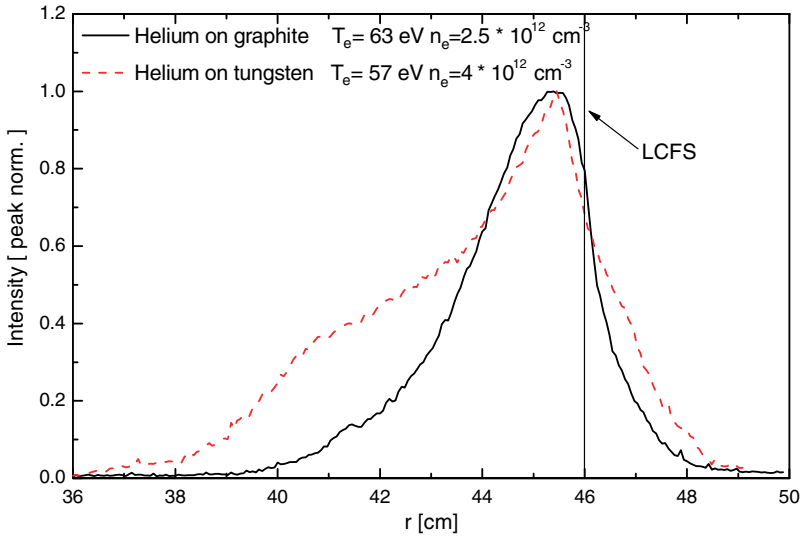

Fig. 6. Radial intensity distribution of He I at the graphite and at the tungsten limiter from the side view of the limiter (LCFS stands for 'Last Closed Flux Surface').

Since the observation volume only covers a part of the hot spots, fast atoms originating from outside may influence the intensity distribution more than the slow ones. Furthermore the probability of emission depends on the local electron density and temperature, which are increasing in the vertical z-direction. This influence is described by the ratio R/z. The z-value is assumed to be 0.3 cm, which is connected to the maximum of the tangential intensity profile (Fig. 3). The chosen Maxwell velocity distribution [13] for thermally desorbed atoms and the Thompson velocity distribution [14] for ion-induced desorption are:

$$f_M = A_1 T_S^{-1/2} \exp\left(-\frac{mv^2}{2k_B T_S}\right) \times \left(1 - \exp\left(-\frac{mv^2}{2k_B T_S}\left(\frac{R}{z}\right)^2\right)\right), \quad (2)$$

$$f_T = A_2 \left(\frac{1}{\left(1 + \left(\frac{v}{v_A}\right)^2\right)^2} - \frac{1}{\left(1 + \left(1 + \left(\frac{R}{z}\right)^2\right)\left(\frac{v}{v_A}\right)^2\right)^2} \right). \quad (3)$$

The free fit parameters are the amplitudes A_1 and A_2, the surface temperature T_S and the velocity v_A which is connected to the activation energy by $v_A = \sqrt{2E_A/m_{He,Ne}}$, for the inert gas. The flux proportionality of the intensity will be taken into account as well as the convolution of the total velocity distribution f_t with the instrument profile A_i.

$$f_t = v(f_M + f_{T_S}), \quad (4)$$

$$F_i = \int_{-\infty}^{\infty} A_i(v - v_0) f_t(v_0) \mathrm{d}v_0. \quad (5)$$

Fig. 7 shows one of the results of a least-square fit. The numerical fit agrees well with the measured data. The determined surface temperatures T_S show good agreement with the thermocouple measured surface temperatures T_T (Fig. 8). The thermocouple is located 5 mm underneath the limiter surface. The surface temperature is obtained from the measured value with the help of the heat transfer equation [22].

The obtained activation energies for helium on graphite surfaces are in the range of 0.7–2 eV. The activation energies are in the same range as those measured under laboratory conditions [15–17]. The activation energy increases with the particle flux. The activation energy of helium in tungsten has been determined to be 2.3 eV. Kornelsen [18] measured an activation energy of $E_A = 2.65$–5.4 eV for a W(1,0,0) tungsten monocrystal and Hino et al. [19] give a value of $E_A = 2.2$ eV. The activation energy of neon in graphite is determined to be 1 eV, which agrees well with the values in [20] (1.1 eV) and [21] (0.4 eV).

The activation energy for neon on tungsten is $E_A = 0.4$ eV, which is clearly smaller than the activation energy of 1–4 eV on a clean monocrystalline tungsten surface reported by Kornelsen [18]. A detailed study of the activation energy in TEXTOR [23] shows a complex behavior that depends on particle flux as well as surface temperature and the complex composition of the surface during the plasma discharge. Nevertheless the activation energies obtained from the measured spectra are in good agreement with the values in the literature.

Concerning the interpretation of the experimental results, especially with respect to particle reflection, the angle of incidence of ions and the ion energy at the surface of the plasma components has a large significance. The angle of incidence

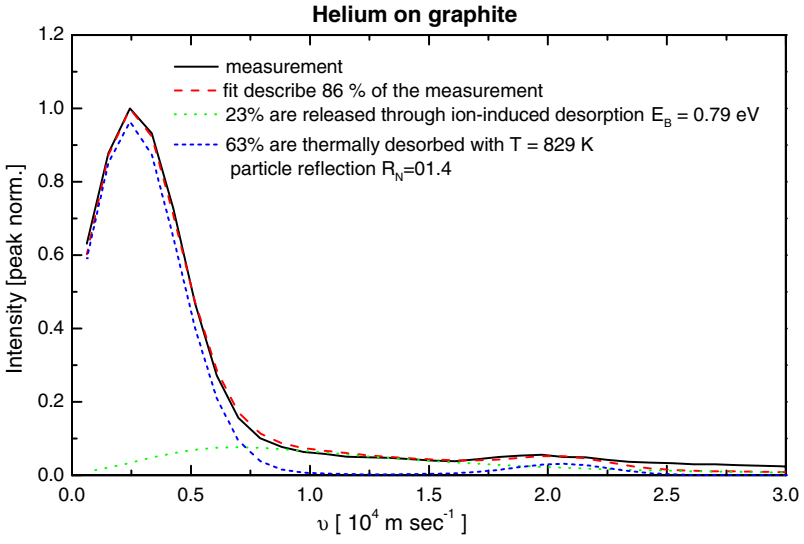

Fig. 7. An example of the fit result.

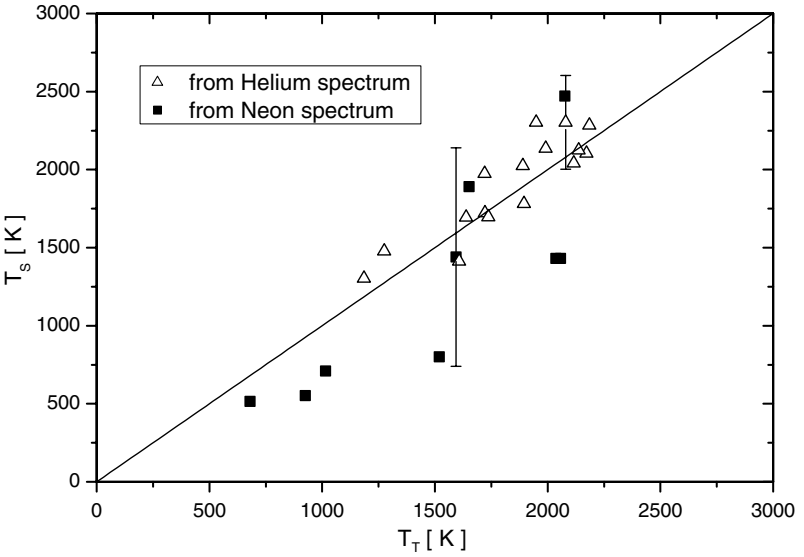

Fig. 8. Limiter surface temperature determined from the Maxwellian velocity distribution compared with the temperature measured with the thermocouple.

and the ion energy have been determined by solving numerically the equation of motion in the magnetic and the Debye sheath [24]. The application of this model to hydrogen ions shows a good agreement with the result obtained in [25]. The result of this numerical calculation for helium, neon and carbon ions is shown in Fig. 9, where α_B is the angle of incidence of the magnetic field lines with respect to the surface normal and γ_i is the angle of incidence of the ions. At the point of observation at the limiter surface the magnetic field line angle is about 70°. This means that the angle of incidence of the helium ions has a value of 50° and that one of neon ions has a value of 60°. The ion energy distribution on the limiter surface is discussed in detail in [24].

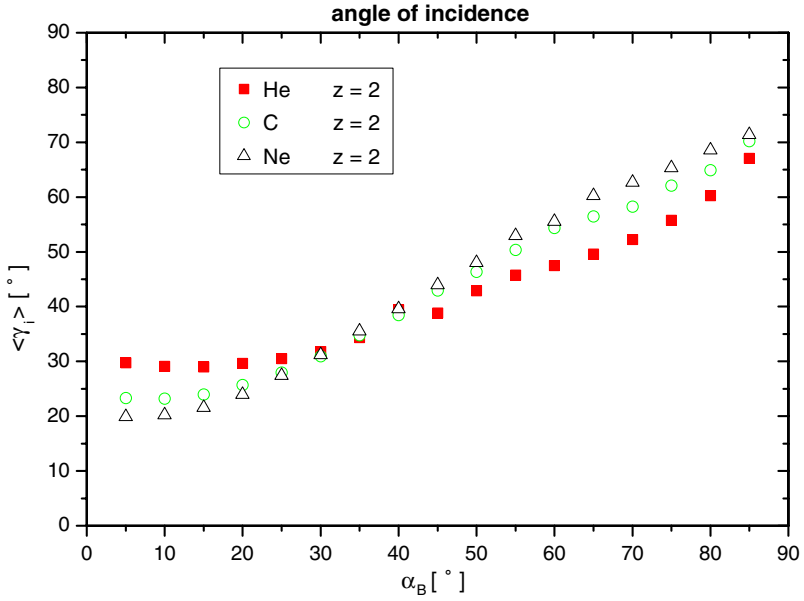

Fig. 9. The average angle of incidence for different species. The plasma parameters are $T_e = 30$ eV, $T_i/T_e = 2$, $n_e = 5 \times 10^{12}$ cm^{-3} and $B = 2.25$ T.

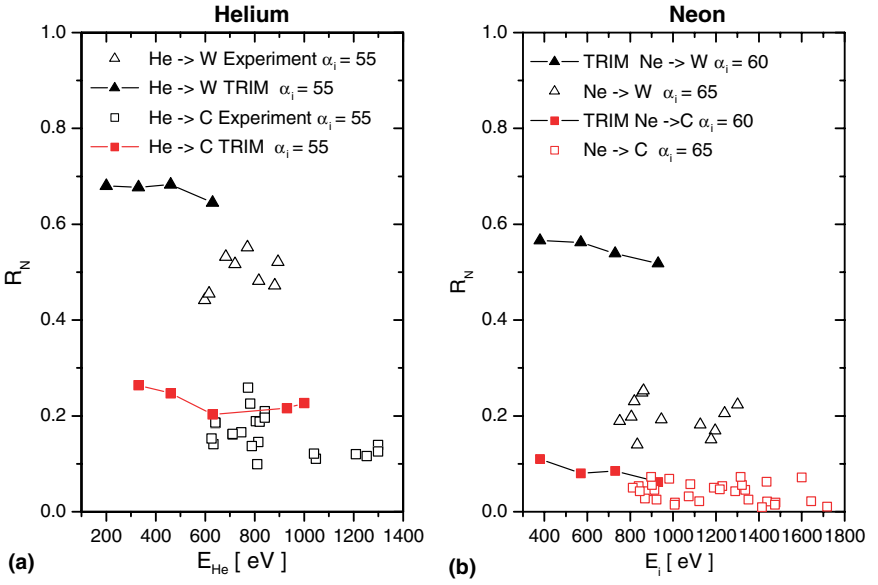

Fig. 10. (a) Particle reflection coefficient of helium on graphite respectively on tungsten. The open symbols are determined with the numerical fit, the close symbols are numerically calculated with TRIM code. (b) A comparison the R_N of neon on graphite and tungsten.

With the assumption that the recycling of the particles is equal to one, the remaining part of the measured intensity distribution can, without a fit to the data, be ascribed to particle reflection. The integral over this part is associated with the particle reflection coefficient R_N. Fig. 10(a) and (b) shows a comparison of experimental values with the numerically calculated ones, which were obtained from the Monte-Carlo code TRIM [7]. The comparison of the particle reflection coefficient shows for helium on graphite surface and neon on graphite surface a good agreement. The calculation of R_N for tungsten shows an overestimation. The reason for this may lie in the coating of the tungsten limiter with carbon during the discharge. This is supported by the fact that the determined R_N of neon is more strongly influenced by the change of surface material than the R_N of helium which agree well with the numerical values Fig. 10(a) and (b).

The penetration of the impurity depends on the velocity distribution as well as on the plasma parameters n_e and T_e, which determine the ionization. Fig. 11(a) shows the average velocity $\langle v \rangle = \frac{\int v f(v) dv}{\int f(v) dv}$ as a function of the electron temperature at the radius of the test limiter. The average velocity decreases only slightly with increasing T_e, in contrast to the electron density n_e which decreases markedly with increasing T_e. On the other hand, a noticeable increase in the thermal load on the limiter

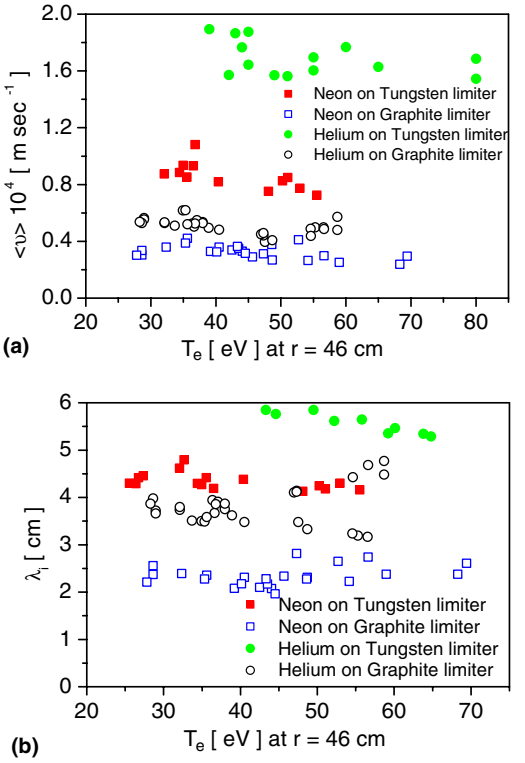

Fig. 11. (a) Mean velocity of helium and neon on graphite and tungsten limiter versus T_e on the LCFS. (b) Penetration depth of helium and neon on graphite and tungsten limiter versus T_e on the LCFS.

can be observed with increasing electron density. This accounts for the somewhat counter–intuitive effect that, on the whole, the observed velocity of released particles increases with decreasing T_e. Helium atoms are 1.7 times faster than neon atoms released from the same target. The average velocity of neon on the tungsten limiter is a factor of four higher than the average velocity of neon on the carbon limiter. Using the measured $f(v)$, n_e- and T_e-profiles are used to calculate the neutral density profile $n_A(r)$ in front of the limiter [10], the resulting ion source distribution $Q(r)$ and the penetration depth λ_i can be calculated according to

$$n_A(r) = n_A(0) \int_0^\infty f(v_A) \exp\left(\frac{1}{v_A} \int_{r_1}^{r_2} n_e(r) \langle \sigma v_e \rangle_i dr\right) dv_A, \tag{6}$$

$$Q(r) = \frac{d\Gamma}{dr} = n_A(r) n_e(r) \langle \sigma v_e \rangle_i(r), \tag{7}$$

$$\lambda_i = \frac{\int Q(r) r dr}{\int Q(r) dr}. \tag{8}$$

The weak dependence of the penetration depth on local plasma parameters, seen in Fig. 11(b), results from two competing processes: with increasing electron density n_e, the temperature decreases and, hence, the ionization rate coefficient $\langle \sigma v_e \rangle$ also decreases in the considered temperature range. On the other hand with decreasing temperature the velocity of the particles increases. The target material plays a role via different energy- and particle-reflection coefficients, which influence the average velocity $\langle v \rangle$.

5. Summary and conclusion

The primary aim of this work was to obtain a quantitative description of plasma wall interaction processes of the noble gases helium and neon with the first wall materials graphite and tungsten. For the first time three different release mechanisms of helium and neon recycling at carbon and tungsten limiters could be distinguished: thermal desorption, ion-induced desorption and particle reflection. Assuming that the thermal desorption is represented by the Maxwellian velocity distribution [5], the ion-induced desorption can be expressed by the Thompson velocity distribution [6] and calculating the particle reflection by the Monte-Carlo code TRIM [7], these three different processes could be identified in the measured intensity distribution.

Within the experimental error bars, the surface temperature as determined from the Maxwellian velocity distribution, is in good agreement with the temperature obtained from thermocouple measurements. The process of ion-induced desorption is determined by the activation energy, which has been found for helium on graphite limiter to be 0.7–2 eV, for helium on tungsten 2.3 eV, for neon on graphite 1 eV and for neon on tungsten 0.4 eV. The particle reflection coefficient for both noble gases at the graphite limiters are well described by TRIM calculations. The measurements of the intensity distributions on the tungsten surface shows an underestimated particle reflection coefficient likely a result of a carbon coating of the limiter. However the numerical quantitative calculations, which take the limiter observation-geometry, the ion energy and the angle of incidence into account describe well the experimental results.

The choice of target material shows the strongest influence on the velocity distributions as well as on the penetration depth. The weak dependence of the penetration depth on the local plasma parameters is due to competing processes: with increasing electron density n_e, the electron temperature decreases and, therefore, the ionization rate coefficient $\langle \sigma v_e \rangle_{ion}$ also decreases. On the other hand with a decreasing temperature the velocity $\langle v \rangle$ of the particles increases. Simultaneous variations of these three factors can compensate, as can be seen from a simplified expression for the penetration depth $\lambda_i = \langle v \rangle / n_e \langle \sigma v_e \rangle_{ion}$, valid for a homogenous plasma (in contrast to Eq. (8) which applies to any plasma profiles).

These results show the importance of the quantitative determination of the release mechanisms of atoms that influence the penetration depth into the plasma.

Acknowledgements

The authors like to acknowledge the support of many fruitful discussions with St. Jachmich and R. Stirn.

References

[1] G. Federici, C.H. Skinner, J.N. Brooks, J.P. Coad, A.A. Haasz, A. Hassanein, V. Philipps, C.S. Pitcher, J. Roth, W.R. Wampler, D.G. Whyte, Nucl. Fusion 41 (12R) (2001) 1967.

[2] H. Bolt, V. Barabash, G. Federici, J. Linke, A. Loarte, J. Roth, K. Sato, J. Nucl. Mater. 307–311 (2002) 43.

[3] G. Janeschitz, J. Nucl. Mater. 290–293 (2001) 1.
[4] ITER Physics Basis, Nucl. Fusion, 39 (1999) p. 2137.
[5] G. Comsa, R. David, Surf. Sci. 117 (1982) 77.
[6] M.W. Thompson, Phil. Mag. 18 (1968) 377.
[7] J.P. Biersack et al., Nucl. Instrum. and Meth. 174 (1980) 257.
[8] B. Schweer et al., Fusion Sci. Technol. 47 (2005) 138.
[9] P. Bogen, E. Hintz, Physics of Plasma-Wall Interaction in Controlled Fusion, in: D.E. Post, R. Behrisch (Eds.), Plenum, New York and London, 1984, p. 211.
[10] A. Pospieszczyk, Atomic and Plasma-Material Interaction Processes in Controlled Thermonuclear Fusion, R.K. Janev, H.W. Drawin (Eds.) (1993) p. 213.
[11] M. Brix, Messung von Elektronentemperaturen und -dichte mittels Heliumstrahldiagnostik im Randschichtplasma von TEXTOR - 94, JÜL-Report 3638 (1999).
[12] S. Brezinsek, A. Huber, Ph. Mertens, A. Pospieszczyk, B. Schweer, G. Sergienko, Fusion Sci. Technol. 47 (2005) 209.
[13] Ph. Mertens et al., J. Nucl. Mater. 128–129 (1984) 551.
[14] P. Bogen et al., J. Nucl. Mater. 145–147 (1987) 434.
[15] S. Tokura et al., J. Nucl. Mater. 155–157 (1988) 246.
[16] H. Atsumi, S. Yamanaka, P. Son, M. Miyake, J. Nucl. Mater. 133–134 (1985) 268.
[17] W. Möller, B.M.U. Scherzer, J. Ehrenberg, J. Nucl. Mater. 111–112 (1982) 669.
[18] E.V. Kornelsen, Can. J. Phys. 48 (1970) 2812.
[19] T. Hino, Y. Yamauchi, Y. Hirohata, J. Nucl. Mater. 266–269 (1999) 538–541.
[20] W. Choi, C. Kim, H. Hang, Surf. Sci. 281 (1993) 323.
[21] C. Brosset, J. Bardon, E. Gauthier, J. Nucl. Mater. 241–243 (1997) 1093.
[22] V. Philipps, private communication.
[23] Y.M. Kim, V. Philipps, M. Rubel, E. Vietzke, A. Pospieszczyk, B. Unterberg, R. Jaspers, J. Vac. Sci. Technol. A 20 (2002) 138.
[24] P. Lindner, H. Gerhauser, H.A. Claaßen, Controlled Fusion and Plasma Physics, Proc. 25th Eur. Conf. (Praha) (1998) p. 1816.
[25] R. Chodura, J. Nucl. Mater. 111–112 (1982) 420.